Molecular Plant Pathology

MOLECULAR PLANT PATHOLOGY (2015) **16**(6), 583–592 DOI: 10.1111/mpp.12215

The xylanase inhibitor TAXI-III counteracts the necrotic activity of a *Fusarium graminearum* xylanase *in vitro* and in durum wheat transgenic plants

ILARIA MOSCETTI[1], FRANCO FAORO[2], STEFANO MORO[3], DAVIDE SABBADIN[3], LUCA SELLA[4], FRANCESCO FAVARON[4] AND RENATO D'OVIDIO[1,*]

[1]*Dipartimento di Scienze e Tecnologie per l'Agricoltura, le Foreste, la Natura e l'Energia (DAFNE), Università della Tuscia, Via S. Camillo de Lellis snc, 01100 Viterbo, Italy*

[2]*Dipartimento di Scienze Agrarie e Ambientali, Università degli Studi di Milano, Via Celoria 2, 20133 Milano, Italy*

[3]*Dipartimento di Scienze del Farmaco, Università degli Studi di Padova, Via Marzolo 5, 35131 Padova, Italy*

[4]*Dipartimento del Territorio e Sistemi Agro-Forestali, Università degli Studi di Padova, Viale dell'Università 16, 35020 Legnaro (PD), Padova, Italy*

SUMMARY

The xylanase inhibitor TAXI-III has been proven to delay Fusarium head blight (FHB) symptoms caused by *Fusarium graminearum* in transgenic durum wheat plants. To elucidate the molecular mechanism underlying the capacity of the TAXI-III transgenic plants to limit FHB symptoms, we treated wheat tissues with the xylanase FGSG_03624, hitherto shown to induce cell death and hydrogen peroxide accumulation. Experiments performed on lemmas of flowering wheat spikes and wheat cell suspension cultures demonstrated that pre-incubation of xylanase FGSG_03624 with TAXI-III significantly decreased cell death. Most interestingly, a reduced cell death relative to control non-transgenic plants was also obtained by treating, with the same xylanase, lemmas of TAXI-III transgenic plants. Molecular modelling studies predicted an interaction between the TAXI-III residue H395 and residues E122 and E214 belonging to the active site of xylanase FGSG_03624. These results provide, for the first time, clear indications *in vitro* and *in planta* that a xylanase inhibitor can prevent the necrotic activity of a xylanase, and suggest that the reduced FHB symptoms on transgenic TAXI-III plants may be a result not only of the direct inhibition of xylanase activity secreted by the pathogen, but also of the capacity of TAXI-III to avoid host cell death.

Keywords: *Fusarium graminearum*, Fusarium head blight, molecular modelling, necrotizing factor, *Triticum durum*, xylanase, xylanase inhibitor.

INTRODUCTION

Plant infection by fungal pathogens is a complex process involving several components. Among these, pathogens secrete cell wall-degrading enzymes (CWDEs) to breach the cell wall barrier and colonize the host tissue (for a review, see Cantu *et al*., 2008). Different classes of CWDEs have been proven to be important factors for successful host tissue colonization. In particular, endo-β-1,4-xylanases (xylanases; EC 3.2.1.8) are key enzymes in the degradation of xylans, a main component of cell walls of commelinoid monocot plants. According to the sequence-based glycoside hydrolase (GH) classification (CAZy classification) (http://www.cazy.org), most xylanases are grouped into families 10 (GH10) and 11 (GH11). A primary role of these enzymes in pathogenesis has been demonstrated for the necrotrophic fungal pathogen *Botrytis cinerea*, as the *Xyn11A* gene was necessary for complete virulence during the infection of tomato leaves and grape berries (Brito *et al*., 2006).

The activity of microbial xylanases is inhibited *in vitro* by specific proteins (xylanase inhibitors, XIs) localized in the plant cell wall (Dornez *et al*., 2010). These inhibitors have been grouped into three different classes: *Triticum aestivum* XI (TAXI) (Debyser *et al*., 1999), xylanase inhibitor protein (XIP) (McLauchlan *et al*., 1999) and thaumatin-like XI (TLXI) (Fierens *et al*., 2007). TAXI-type and TLXI-type inhibitors inhibit xylanases of the GH11 family, whereas XIP-type inhibitors inhibit xylanases of the GH10 and GH11 families. XIs are considered to be part of the defence mechanisms used by plants to counteract microbial pathogens because of their capacity to inhibit specifically microbial xylanases and additional features, including their induction following pathogen infection. For example, *Taxi-III* is poorly accumulated in spike tissue, but is strongly induced by *Fusarium graminearum* infection, the causal agent of the devastating Fusarium head blight (FHB) disease of wheat and barley (Igawa *et al*., 2004; Moscetti *et al*., 2013). Recently, we have provided evidence *in planta* for the protective role of TAXI-III (Moscetti *et al*., 2013) against *F. graminearum* infection. Indeed, wheat transgenic plants constitutively expressing TAXI-III showed a delay of FHB symptoms and a reduced accumulation of fungal biomass in their caryopses (Moscetti *et al*., 2013). Furthermore, the protective role of XI has been recently extended to insects in rice (Xin *et al*., 2014).

**Correspondence*: Email: dovidio@unitus.it

Fungal xylanases can also induce necrosis and activate defence responses in plants. This capacity is unrelated to their enzymatic activity (Enkerli *et al*., 1999; Furman-Matarasso *et al*., 1999; Noda *et al*., 2010; Sharon *et al*., 1993), and is caused by a short stretch of amino acids on the enzyme surface, as shown for EIX and Xyn11A of *Trichoderma viride* and *Botrytis cinerea*, respectively (Noda *et al*., 2010; Rotblat *et al*., 2002). It has also been shown that the short amino acid stretch (TKLGE) in the EIX enzyme is essential for recognition by a leucine-rich receptor (LRR)-like protein in tomato (Ron and Avni, 2004), whereas a 30-amino-acid peptide in Xyn11A mediates binding to tobacco spheroplasts (Noda *et al*., 2010).

Recently, one of the most expressed GH11 xylanases of *F. graminearum*, the xylanase FGSG_03624, has been shown to induce cell death and hydrogen peroxide accumulation in wheat tissues. This property was hypothesized to be connected to the presence of a short stretch of amino acids with some similarity to those reported to be essential for the elicitation of the necrotic responses by the xylanases EIX and Xyn11A of *T. viride* and *B. cinerea*, respectively (Sella *et al*., 2013).

In order to verify whether TAXI-III can affect the capacity of this enzyme to induce cell death, we treated wheat lemmas or wheat cell suspensions with the xylanase FGSG_03624 pre-incubated with purified TAXI-III. Moreover, we performed experiments with FGSG_03624 on lemmas of transgenic wheat plants expressing TAXI-III. Finally, we propose a molecular model for the interaction between TAXI-III and the xylanase FGSG_03624.

RESULTS

TAXI-III limits plant cell death caused by a *F. graminearum* xylanase in lemma tissues

As spikelets are the preferred penetration sites of *F. graminearum*, we performed histochemical analyses on wheat lemmas of durum wheat cv. Svevo. Purified FGSG_03624 xylanase (0.2 μg) was mixed with purified TAXI-III (0.3 μg), and the mixture was used to treat wheat lemmas. Treatment with FGSG_03624 alone was used as a control. The amount of TAXI-III used (0.3 μg) was sufficient to inhibit to completion the activity of FGSG_03624 xylanase (Fig. 1). As the heat-inactivated xylanase induces necrosis (Sella *et al*., 2013), we also performed treatments with boiled FGSG_03624 in the presence and absence of TAXI-III. Microscopic analysis of durum wheat lemmas treated with the xylanase, in both native and boiled forms, showed the occurrence of cell death, as revealed by trypan blue vital staining (Fig. 2c,e). The quantification of dead cells by image analysis of digitalized micrographs indicated that boiled xylanase was slightly less effective in inducing cell death, although this difference was not significant (Fig. S1, see Supporting Information). However, lemmas treated with either native or boiled FGSG_03624 xylanase co-incubated with TAXI-III showed significant reduction in cell death (Figs 2d,f and S1). Lemmas treated with buffer only or with TAXI-III alone showed only a few scattered dead cells (Figs 2a,b and S1).

The effect of TAXI-III in reducing cell death caused by a *F. graminearum* xylanase is also evident in undifferentiated wheat cell suspension

To verify whether the necrotic activity of the xylanase FGSG_03624 was limited to differentiated tissue or would also affect undifferentiated cells, we treated wheat cell suspensions with this enzyme and determined the percentage of dead cells using the vital stain trypan blue. Cell suspensions in exponential growth phase were treated with three different amounts of FGSG_03624 for 24 h. Untreated cells or cells treated with buffer only were used as negative controls and showed similar cell death values, indicating that buffer does not affect cell vitality (Fig. 3). Conversely, cell suspensions treated with the xylanase FGSG_03624 showed a significant increase in cell death compared with untreated samples or samples treated with buffer only. In particular, the percentage of cell death was significantly higher with a larger amount of xylanase, i.e. approximately 22% and 32% with 0.2 and 3 μg of xylanase, respectively. However, treatments with 1 and 3 μg of xylanase did not differ significantly (Fig. 3a).

On the basis of these results, we performed analogous experiments by treating cell suspensions with FGSG_03624 (1 μg) in the absence or presence of purified TAXI-III (1.5 μg). Treatments with xylanase or boiled xylanase caused 33.5% and 31.4% of dead cells, respectively, whereas co-incubation of TAXI-III with the xylanase or the boiled xylanase prior to the addition to the cell suspensions significantly reduced the number of dead cells to 18.7% and 20.6%, respectively (Fig. 3b).

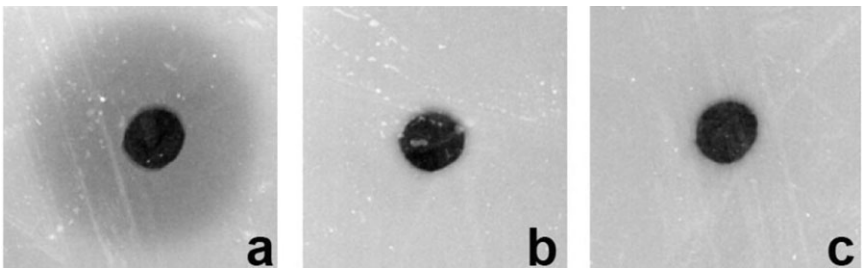

Fig. 1 Inhibition of FGSG_03624 xylanase activity by TAXI-III. The radial gel diffusion assay was performed with FGSG_03624 xylanase (0.2 μg) (a), FGSG_03624 xylanase (0.2 μg) co-incubated with TAXI-III (0.3 μg) (b) and boiled FGSG_03624 xylanase (0.2 μg) (c). The absence of a halo indicates the lack of xylanase activity.

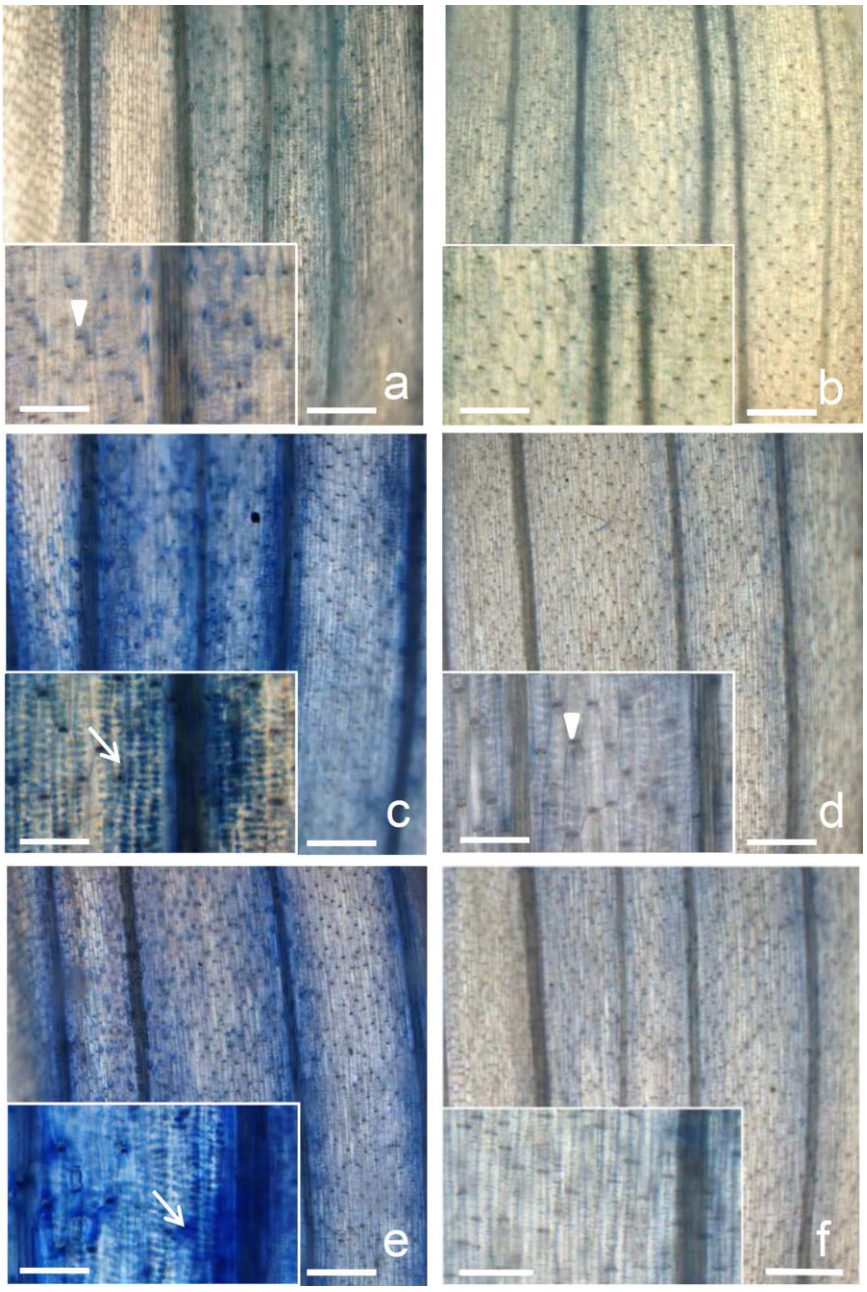

Fig. 2 Killing effect of FGSG_03624 xylanase on lemma tissues of wheat spikelets and capacity of TAXI-III to reduce this effect. The tissue was treated with 10-μL droplets of phosphate-buffered saline (PBS) alone as control (a), or containing 0.3 μg of TAXI-III (b), 0.2 μg FGSG_03624 xylanase (c), the same amount of xylanase boiled for 30 min (e), or the same amount of native and boiled xylanase co-incubated with 0.3 μg TAXI-III (d and f, respectively), and stained after 24 h with trypan blue to detect dead cells (arrows). Many mesophyll cells in the areas treated with both non-boiled (c) and boiled (e) xylanase are dead (30.73 ± 6.35 and 20.16 ± 4.52, respectively), whereas those treated with both non-boiled (d) and boiled (f) xylanase co-incubated with TAXI-III show only a few damaged cells (5.57 ± 1.41 and 7.2 ± 3.37, respectively) and are not significantly different from controls treated with buffer only (a) or TAXI-III only (b) (4.54 ± 1.15 and 7.31 ± 3.4, respectively); the dark spots represent trichome cells (arrowheads); all bars represent 500 μm, except for those in the insets which represent 50 μm. The above-specified values in parentheses represent the percentage of dead cells ± standard deviation (SD) per square centimetre of lemma tissue at 40× magnification.

These results confirmed those obtained on wheat lemmas with regard to the capacity of TAXI-III to limit cell death caused by the xylanase FGSG_03624, and extended the capacity of this enzyme to elicit cell death also in undifferentiated wheat cells.

Lemmas of transgenic plants expressing TAXI-III show reduced cell death caused by a *F. graminearum* xylanase

On the basis of the above results, we verified the effect of xylanase FGSG_03624 on tissues of transgenic wheat plants expressing TAXI-III. In these experiments, purified FGSG_03624 xylanase (0.2 μg) or the same heat-inactivated enzyme was used to treat lemmas of TAXI-III plants and control wild-type plants. As expected, the FGSG_03624 xylanase and its boiled sample caused cell death on lemmas of wild-type plants, as indicated by the blue-stained tissue treated with trypan blue (Fig. 4c,e). Conversely, cell death was almost completely abolished on lemmas of TAXI-III plants treated with FGSG_03624 xylanase or the boiled sample (Fig. 4d,f). Quantification analysis of cell death in the different treatments showed about 85% signal intensity reduction in the TAXI-III plants compared with control plants (Fig. S2, see Supporting Information).

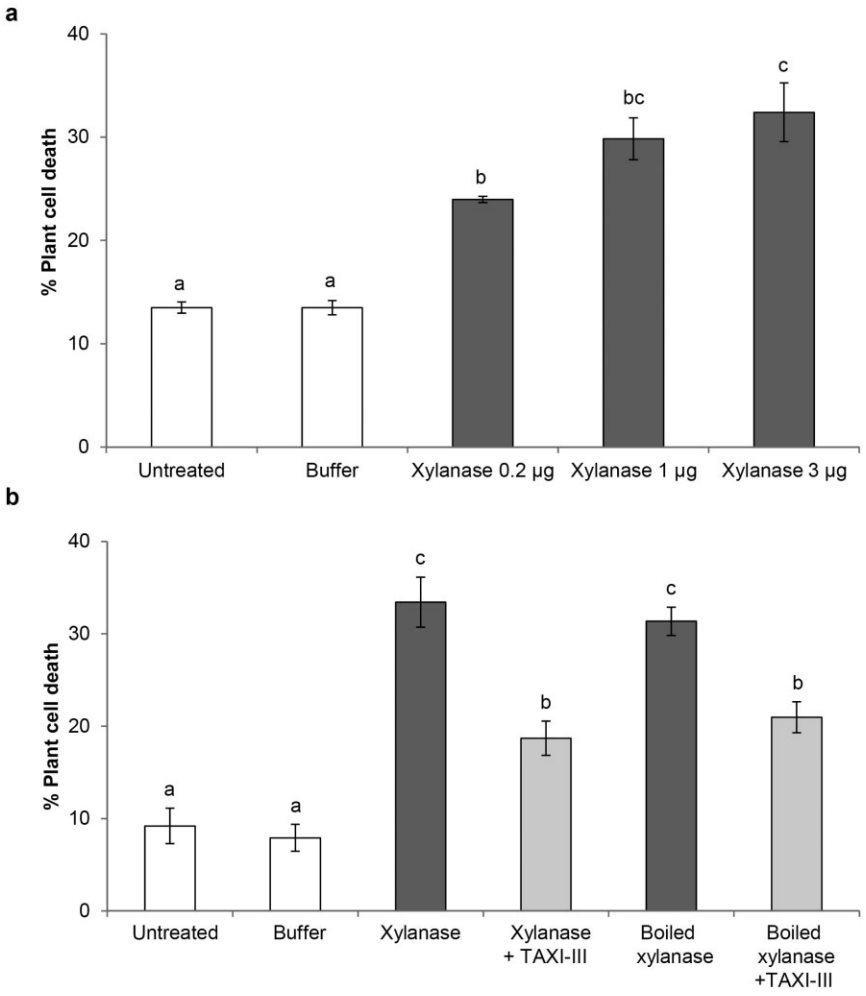

Fig. 3 Effect of FGSG_03624 xylanase on the death of wheat cell suspensions and capacity of TAXI-III to reduce cell death. (a) Cells (200 μL) treated with increasing xylanase amounts (from 0.2 to 3 μg). (b) Cells treated with 1 μg of xylanase and 1.5 μg of TAXI-III. Untreated cells and cells treated with buffer only were used as negative controls. Data were subjected to one-way analysis of variance (ANOVA) and, when a significant *F* value was observed, a pairwise analysis at the 0.95 confidence level was carried out by the Duncan test.

TAXI-III and control plants show similar levels of expression of *TaPr-1*, *TaDAD2* and *TaMCA4* genes

In order to verify whether the expression of *Taxi-III* in the transgenic plants modified the expression pattern of genes related to the defence response and cell death, quantitative reverse transcriptase-polymerase chain reaction (qRT-PCR) analyses of the pathogenesis-related gene *TaPr-1* (*Pr*, *pathogenesis-related*) and of the *TaDAD2* (*DAD*, *defender against cell death*) and *TaMCA4* (*MCA*, *metacaspase*) genes related to cell death were performed. We also verified the expression level of the *Taxi-III* gene by performing qRT-PCR with primers Taxi-III170F/Taxi-III5R. As expected from our previous report (Moscetti *et al*., 2013), *Taxi-III* was strongly expressed in the transgenic wheat spikelets with an approximately 500-fold increase (543.72 ± 29.28) compared with the wild-type control plants. On the contrary, qRT-PCR analyses of *TaPr-1* (1.84 ± 0.20), *TaDAD2* (1.54 ± 0.46) and *TaMCA4* (1.63 ± 0.44) genes showed no significant difference in the expression levels between transgenic and wild-type plants.

Molecular modelling studies show that TAXI-III can interact with the active site of the *F. graminearum* xylanase

In order to elucidate the molecular bases responsible for the capacity of TAXI-III to inhibit the activity and necrotizing capacity of the xylanase FGSG_03624, we reconstructed the hypothetical three-dimensional structure of TAXI-III complexed with xylanase FGSG_03624 using a conventional homology modelling approach. Among the available crystallographic templates, we selected the structure of TAXI-IIA complexed with *Bacillus subtilis* xylanase (PDB code: 3HD8) and the crystal structure of TAXI-I complexed with *B. subtilis* xylanase (PDB code: 2B42), considering as acceptable the sequence similarity (higher than 70%) of the two complexes, as described previously (Pollet *et al*., 2009). The overall structure of TAXI-III complexed with xylanase FGSG_03624 is shown in Fig. 5 and, not surprisingly, the energetically more stable structural organization of TAXI-III complexed with xylanase FGSG_03624 presents a highly similar architecture to the structure

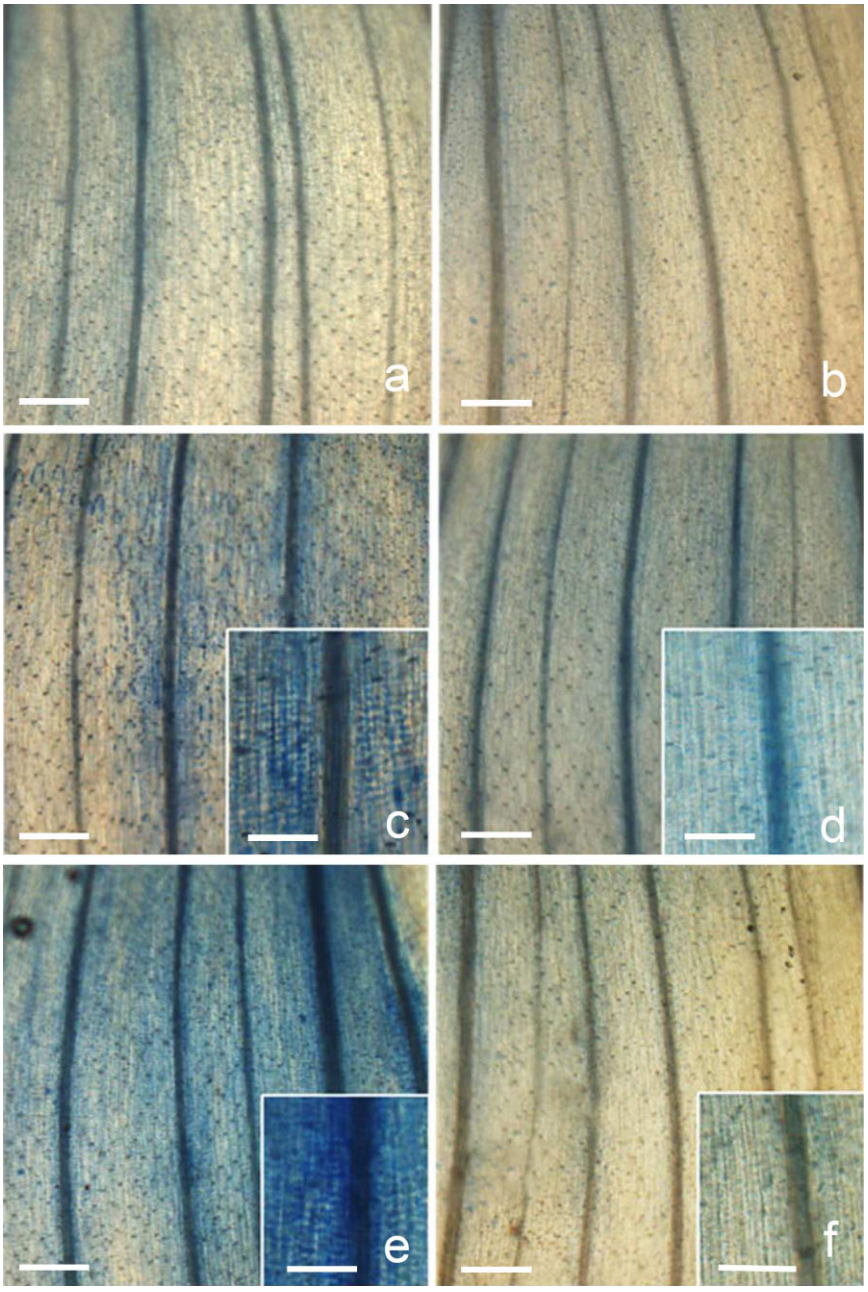

Fig. 4 Capacity of TAXI-III plants to reduce cell death of wheat tissue. Lemmas of wheat control plants (left) and TAXI-III plants (right) were treated with phosphate-buffered saline (PBS) as a control (a, b), or 0.2 μg of FGSG_03624 xylanase (c, d) or the same amount of xylanase boiled for 30 min (e, f), and stained after 24 h with trypan blue to detect dead cells. Many mesophyll cells in lemmas of control plants treated with both non-boiled (c) and boiled (e) xylanase are dead (33.51 ± 2.43 and 34.39 ± 3.08, respectively), whereas lemmas of TAXI-III plants treated with xylanase (d) or boiled xylanase (f) show significant reduction of cell death values (5.11 ± 1.79 and 5.24 ± 1.48, respectively), as do lemmas treated with buffer only (a, b) (10.49 ± 3.62 and 8.97 ± 1.96, respectively); all bars represent 500 μm, except for those in the insets which represent 50 μm. The above-specified values in parentheses represent the percentage of dead cells ± standard deviation (SD) per square centimetre of lemma tissue at 40× magnification.

of both templates [pairwise Cα root-mean-square difference (RMSD) over 560 residues, 2.33 Å; Fig. S3, see Supporting Information]. In particular, in the modelled structure of TAXI-III complexed with xylanase FGSG_03624, the imidazole side-chain of $His395_{TAXI\text{-}III}$ is located directly between the two catalytic glutamate (Glu) residues (Glu122 and Glu214) of FGSG_03624 xylanase, as detailed in Fig. 5. Interestingly, in this position, the $N^{\varepsilon 2}$ atom of the imidazole side-chain is stabilized through hydrogen-bonded contacts with the oxygen atom of $Glu172_{XYL}$ (3.1 Å). Another possible stabilizing interaction, preferably mediated by a water molecule, is with the negatively charged oxygen of $Glu112_{XYL}$. This interaction scheme has also been proposed to describe the structural basis of inhibition of *B. subtilis* xylanase by TAXI-IA and TAXI-IIA (Pollet *et al*., 2009). Accordingly, the general interactive scheme described by Pollet *et al*. (2009) is pretty well conserved, and it is worth emphasizing that the interaction of residues Leu292 of TAXI-I and Pro294 of TAXI-IIA with the -2 glycon subsite of the xylanase (critical for both inhibition strength and specificity) is guaranteed by Leu294 of TAXI-III. In this interaction scheme, TAXI-III does not interact with the short stretch of residues 139–149 (QKKGEINIDGS), suggested by Sella *et al*. (2013) to be involved in the necrotizing activity of FGSG_03624.

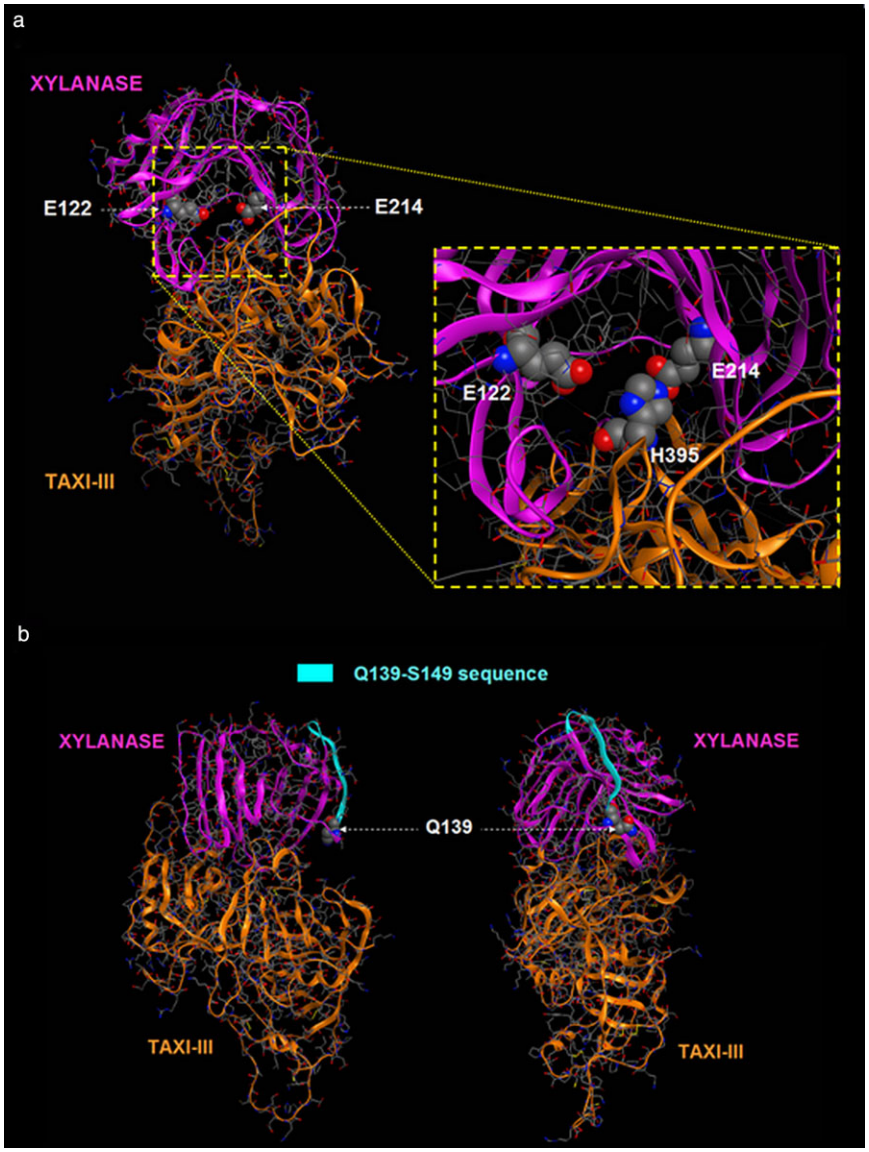

Fig. 5 Overall structure of the homology modelling complex of TAXI-III/xylanase FGSG_03624. (a) The interaction scheme between His395TAXI-III and the two catalytic glutamate residues (Glu122 and Glu214) of FGSG_03624 xylanase. (b) In cyan, the short stretch of residues 139–149 (QKKGEINIDGS) possibly involved in the necrotizing activity of FGSG_03624 (Sella *et al*., 2013). There is an appreciable lack of interaction of this region of xylanase with TAXI-III.

DISCUSSION

We have shown previously that the reduction of FHB symptoms observed in TAXI-III plants is related to the capacity of TAXI-III to inhibit the xylanase activity of the causal agent *F. graminearum*. Indeed, the finding that TAXI-III did not inhibit the xylanase activity of *Bipolaris sorokiniana* was in agreement with the inability of TAXI-III plants to reduce leaf blotch symptoms caused by this fungus (Moscetti *et al*., 2013).

To shed further light onto the molecular mechanism underlying the capacity of the transgenic plants expressing TAXI-III to limit FHB disease symptoms, we performed experiments with the xylanase FGSG_03624, which has been shown previously to cause plant cell death in wheat tissues (Sella *et al*., 2013). Our results showed that the co-incubation of TAXI-III with the xylanase prior to treatment prevented cell death of wheat lemma tissue. This protective action of TAXI-III was also evident on wheat cell suspensions treated with the xylanase FGSG_03624. In these experiments, the percentage of cell death was dependent on the amount of xylanase used in the treatments, and co-incubation with TAXI-III reduced cell death by about 40%. More interestingly, the capacity of the xylanase FGSG_03624 to cause cell death was clearly reduced on lemmas of transgenic wheat plants expressing TAXI-III.

The above results and the lack of significant alterations in gene expression in TAXI-III plants, as indicated by the pathogenesis-related *TaPr1* gene and by the *TaDAD2* and *TaMCA4* genes related to cell death, suggest that the delay of FHB symptoms on transgenic TAXI-III plants may be a result of the capacity of TAXI-III to inhibit fungal xylanase activity and/or to prevent the cell death induced by the xylanase FGSG_03624.

On the basis of the sequence similarity between the xylanases FGSG_03624, EIX of *T. viride* and Xyn11A of *B. cinerea* (Noda *et al*., 2010; Rotblat *et al*., 2002), we have proposed previously that the cell death activity of FGSG_03624 is caused by a short stretch of amino acids (QKKGEINIDGS, 139–149) on the enzyme surface (Sella *et al*., 2013). Both EIX and Xyn11A xylanases have been shown to bind to the plasma membrane and, for the former xylanase, a plasma membrane receptor protein essential for cell death elicitation has been identified (Ron and Avni, 2004). On the basis of this finding, Noda *et al*. (2010) proposed that the xylanase Xyn11A acts as a pathogen-associated molecular pattern (PAMP) to induce the hypersensitive response (HR) during the infection of the necrotrophic fungus *B. cinerea*. This type of host response, instead of limiting pathogen colonization, as in the case of infection caused by biotrophs, would facilitate *B. cinerea* infection (Govrin and Levine, 2000), and probably represents a mechanism actively induced by necrotrophs. Recently, in support of this hypothesis, a number of effector candidates have been identified using bioinformatics approaches in the necrotrophic fungal pathogen *Sclerotinia sclerotiorum*, one of which encodes a putative xylanase (Guyon *et al*., 2014).

In this context, the occurrence of XIs may counteract the action of xylanase in inducing cell death and disease development. Our molecular modelling studies predict that TAXI-III interacts with the two catalytic Glu residues at positions 122 and 214 of the active site of FGSG_03624, providing support for the capacity of this inhibitor to hinder the xylanase activity of *F. graminearum*. However, this interaction scheme did not highlight any interaction between TAXI-III and the short stretch of residues (139–149, QKKGEINIDGS) possibly involved in the necrotizing activity of FGSG_03624 (Sella *et al*., 2013). This finding raises the question of whether the cell death activity of FGSG_03624 is caused by the proposed peptide 139–149 or whether it is located in another region of the protein. However, the observation that the capacity of TAXI-III to prevent cell death persists, even after treatment with boiled xylanase, suggests that this capacity is not affected by changes in the xylanase structure, including the destruction of the active site. These results are in agreement with previous reports on the cell death activity of EIX and Xyn11A xylanases of *T. viride* and *B. cinerea*, respectively (Noda *et al*., 2010; Rotblat *et al*., 2002), because, in both cases, the capacity to induce necrosis is unrelated to their enzymatic activity (Enkerli *et al*., 1999; Furman-Matarasso *et al*., 1999; Noda *et al*., 2010; Sharon *et al*., 1993). Moreover, based on the results with the EIX enzyme, whose necrotizing peptide binds to an LRR-like protein (Ron and Avni, 2004), we hypothesize that the ability of TAXI-III to prevent cell death may be a result of its capacity to preclude the binding of FGSG_03624 xylanase to a putative plant receptor.

The possibility that TAXI-III can exert a dual activity to counteract pathogen infection is not novel for glycosidase inhibitors of CWDEs produced by fungal pathogens. Indeed, the polygalacturonase-inhibiting protein (PGIP), which inhibits fungal polygalacturonase (PG) activity (De Lorenzo *et al*., 2001), has been shown to prevent cell death activity displayed by a PG of the fungal pathogen *Sclerotinia sclerotiorum*. This capacity has been shown for the soybean PGIP (Zuppini *et al*., 2005) and for the *Brassica napus* PGIP (Bashi *et al*., 2013). In the latter case, the capacity of this inhibitor to reduce necrosis correlates with the delay of disease symptoms caused by *S. sclerotiorum* in transgenic Arabidopsis plants (Bashi *et al*., 2013).

Although several findings indicate the importance of the xylanase FGSG_03624 in pathogenesis, knockout experiments have shown that its presence is not essential for the virulence of *F. graminearum* (Sella *et al*., 2013). This aspect can be explained by considering that the pathogen produces at least six xylanases during the infection process (Sella *et al*., 2013) and the lack of a single xylanase gene could be replaced by the redundant function of the other xylanases. However, TAXI-III is active against two of these enzymes (Moscetti *et al*., 2013), and this multiple interaction may explain why TAXI-III plants show reduced FHB symptoms (Moscetti *et al*., 2013).

In conclusion, we provide, for the first time, clear indications that an XI can prevent the necrotic activity of a xylanase. We also suggest that TAXI-III can contribute to the delay of the FHB symptoms observed in TAXI-III plants by inhibiting the hydrolytic activity of the xylanases secreted by the pathogen and/or by preventing the necrotizing activity of the xylanase FGSG_03624.

EXPERIMENTAL PROCEDURES

Plant growth

Wheat seeds of *T. durum* cv. Svevo and transgenic *T. durum* cv. Svevo expressing TAXI-III (Moscetti *et al*., 2013) were surface sterilized with sodium hypochlorite (0.5%, v/v) for 10 min and then rinsed thoroughly in sterile water. Plants were vernalized at 4 °C for 2 weeks and grown in a climatic chamber at 18–23 °C with a 14-h photoperiod (300 $\mu E/m^2/s$). The wheat growth stages were based on the method of Zadoks *et al*. (1974).

TAXI-III and xylanase FGSG_03624 purification

TAXI-III extraction and purification were performed as reported in Moscetti *et al*. (2013). Briefly, crude protein extracts from leaves of TAXI-III plants were obtained by homogenizing wheat tissues in the presence of McIlvaine buffer at pH 5.0 (0.2 M disodium hydrogen phosphate and 0.1 M citric acid). The homogenate was shaken for 1 h at 4 °C and centrifuged for 20 min at 10 000 ***g***. The supernatant was recovered and TAXI-III was purified by affinity chromatography on a xylanase–Sepharose conjugate column.

Xylanase FGSG_03624 was purified as reported by Sella *et al*. (2013).

Protein concentrations were determined using the Bio-Rad Protein assay kit (Bio-Rad Laboratories, Segrate, Italy) following the manufacturer's protocol, and by sodium dodecylsulfate polyacrylamide gel electrophoresis (SDS-PAGE) analysis.

Xylanase activity and inhibition assays

The enzyme activity of the purified xylanase FGSG_03624 and the inhibition activity of purified TAXI-III were measured by radial gel diffusion assay or by using the 2,4-dinitrosalicyclic acid (DNS) assay, as reported in Moscetti *et al*. (2013).

Histochemistry of wheat tissues treated with FGSG_03624 xylanase

Lemma tissues excised from durum wheat spikelets at the anthesis stage were treated with a 10-μL drop containing purified FGSG_03624 (20 ng/μL) (Sella *et al*., 2013), or the same amount of xylanase boiled for 30–45 min to destroy its enzymatic activity, or the above-mentioned xylanases co-incubated for 10 min with TAXI-III purified protein (0.3 μg), or with TAXI-III only. Phosphate-buffered saline (PBS), 0.01 M, pH 7.4, was used to bring samples to final volume and as a negative control.

The xylanase activity, its inactivation in boiled samples and the inhibition of activity after co-incubation with TAXI-III were tested using radial gel diffusion assay.

A 10-μL drop of one of the previously described samples was placed on the surface of a detached lemma and the tissues were incubated for 24 h in a humid chamber. Staining was performed with trypan blue (1 mg/mL; Sigma-Aldrich, Milan, Italy) to detect cell death, as detailed in Faoro and Iriti (2005).

The same treatment with the FGSG_03624 xylanase in native and boiled form was also performed using lemmas from TAXI-III plants and from wild-type plants as controls, employing the same staining conditions.

All samples were examined with an Olympus BX50 light microscope (Olympus, Tokyo, Japan), equipped with differential interference contrast (DIC), epipolarization filters and a Retiga-2000R CCD camera (Q-imaging, Surrey, BC, Canada). Digitalized images were analysed by Photoshop to quantify the number of damaged/dead cells (see details in Faoro and Iriti, 2005). Data were subjected to one-way analysis of variance (ANOVA) and, when a significant *F* value was observed, a pairwise analysis at the 0.95 confidence level was carried out by the Duncan test.

Cytochemistry of wheat cells treated with FGSG_03624 xylanase

Cell line PC998 (*Triticum aestivum* L. emend. Fiori et Paol. cv. Heines Koga II) (DSMZ-Deutsche Sammlung von Mikro-organismen und Zellkulturen GmbH, Braunschweig, Germany) was grown in suspension culture in Gamborg's B-5 Basal Medium with Minimal Organics (Sigma-Aldrich) supplemented with 20 g/L sucrose, adjusted to pH 5.5 and sterilized at 121 °C for 20 min. After autoclaving, 2,4-Dichlorophenoxyacetic acid (2,4-D; 2 mg/L) was added to maintain callus proliferation.

Cell suspensions were grown in dark conditions at 23 °C on a gyratory shaker at 100 rpm. For propagation, every 15 days, 25 mL of fresh medium were added to 25 mL of old culture, mixed and divided equally into two 125-mL Erlenmeyer flasks. For cytochemical experiments, a cell suspension was sampled from a 7-day-old subculture in exponential growth phase, and 200 μL were aliquoted into each 1.5-mL tube. Each sampling tube was inoculated with the FGSG_03624 xylanase (1 μg) or the same amount of FGSG_03624 xylanase boiled for 40 min or the above-mentioned xylanases singularly co-incubated with TAXI-III (1.5 μg) for 10 min at room temperature. Negative controls were the xylanase elution buffer, the TAXI-III elution buffer and untreated cells. Boiled cells (10 min at 100 °C) used as positive control produced, on average, about 50% of dead cells. Sample treatments and staining were based on the procedure reported by Iriti *et al*. (2006). Each sample was incubated at 23 °C, 100 rpm for 24 h, and then stained with 1 mL of trypan blue (0.15 mg/mL) in distilled water for 10 min. Cells were sedimented at 1000 ***g*** for 3 min, washed twice with distilled water and resuspended in 20 μL of distilled water for microscopic analysis. One hundred cells for each sample were counted from 10 microscopic fields selected at random, recording the blue-stained and unstained cells. Blue staining, caused by membrane permeabilization, revealed dead cells. Two biological and six technical replicates for each sample were analysed. Data were subjected to ANOVA and, when a significant *F* value was observed, a pairwise analysis at the 0.95 confidence level was carried out by the Duncan test.

All samples were examined with a Leica DM5000B microscope (Leica Microsystems, Milan, Italy) using bright field transmitted light.

qRT-PCR analyses

Total RNA was extracted from adult plants using the RNeasy plant mini kit (Qiagen, Milan, Italy) according to the manufacturer's instructions. qRT-PCR experiments were performed using the iCycler (Bio-Rad Laboratories, Monza, Italy) and the master mix iQTMSYBR Green supermix (Bio-Rad Laboratories) containing the flurogenic SYBR Green I DNA binding dye. The oligonucleotide primer pairs used were Taxi III 170F (5'-GTCCACGT GCGAGGGTAGT) and Taxi III 5R (5'-CG GGTGTTCTCCACTTTGAT) for *Taxi-III*, and Taact77F (5'-TCCTGTGTTGCTGACTGAGG) and Taact312R (5'-GGTCCAAACGAAGGATAGCA) for Actin (accession number AB181991). The homologous genes *TaPr-1-1/2/3*, located on the short arm of wheat homologous group 5 (Lu *et al*., 2011), were simultaneously amplified using previously developed primers for *PR1.1* (Lu *et al*., 2006). The *TaDAD2* gene was amplified using the primers previously reported by Wang *et al*. (2011), and the *TaMCA4* gene (Wang *et al*., 2012; accession number JN807891) was amplified using the primers TaMCA4 712F (5'-TCAATCCGGCTGACTCTGTT) and TaMCA4 994R (5'-CACTGATGAGGAT GCCGTTG).

The specificity of the primers was verified by nucleotide sequencing of the specific amplicon. The Actin gene was used as housekeeping gene. The total reaction volume was 15 μL and included 7.5 μL of (2×) MasterMix, 100 ng of cDNA, 0.5 μL of 10 μM of each forward and reverse primer, with the volume adjusted with water. Each reaction was performed in triplicate. Reaction conditions were as follows: one cycle at 50 °C for 2 min and 95 °C for 5 min, followed by 40 cycles at 95 °C for 40 s, 61 °C for 40 s and 72 °C for 40 s, and, finally, 90 cycles at 55 °C for 10 s, increasing the set point temperature after cycle 2 by 0.5 °C. The relative expression analysis was determined using the $2^{-\Delta\Delta Ct}$ method (Livak and Schmittgen, 2001) (User Bulletin Number 2-P/N 4303859; Applied Biosystems, Foster City, CA, USA). Calculation and statistical analyses were performed by Gene Expression Macro Version 1.1 (Bio-Rad Laboratories). The qRT-PCR experiments were performed on RNA samples from two different biological replicates.

ΔCt values of control and Taxi-III plants were subjected to statistical analysis applying Student's *t*-test.

Molecular modelling of the interaction between TAXI-III and FGSG_03624

The crystallographic structures of TAXI-I and TAXI-IIA complexed with *B. subtilis* xylanase were retrieved from the Protein Data Bank, PDB codes 2B42 and 3HD8, respectively (Pollet *et al*., 2009). Hydrogen atoms were added using standard geometries to the protein structure with the Molecular Operation Environment program (MOE, version 2013.08; Chemical Computing Group Inc., Montreal, QC, Canada). The hypothetical three-dimensional structure of TAXI-III complexed with the xylanase FGSG_03624 was carried out using a conventional homology modelling approach implemented in the MOE suite, and using both 2B42 and 3HD8 crystallographic structures as structural templates. Specifically, 55 independent intermediate models were constructed by the Boltzmann-weighted randomized modelling procedure. Each was submitted to an electrostatics-enabled minimization run which terminates when the gradient falls below the preselected RMS of the conjugate gradient value (<0.5 kcal/mol/Å). The final model was selected from the intermediate model ensemble using as scoring function the Coulomb and generalized Born interaction energies of the model (Labute, 2009).

To appropriately assign ionization states and hydrogen positions, we used the 'Protonate-3D' tool implemented by MOE (Labute, 2009). To minimize contacts among hydrogen atoms, the structures were subjected to Amber99 (Hornak *et al*., 2006) force field minimization until the RMS of the conjugate gradient was <0.1 kcal/mol/Å, keeping the heavy atoms fixed at their crystallographic positions. The model was inspected using MOE's Protein Geometry stereochemical quality evaluation tools in order to confirm that the model's stereochemistry is reasonably consistent with typical values found in crystal structures.

ACKNOWLEDGEMENTS

This research was supported by the Italian Ministry of University and Research (PRIN 2010–2011) to RD. The molecular modelling work coordinated by SM was carried out with financial support from the University of Padova, Italy and the Italian Ministry for University and Research. We are very grateful to the Chemical Computing Group for the long and fruitful collaboration. We acknowledge Carla Castiglioni for useful assistance in xylanase purification.

REFERENCES

Bashi, Z.D., Rimmer, S.R., Khachatourians, G.G. and Hegedus, D.D. (2013) *Brassica napus* polygalacturonase inhibitor proteins inhibit *Sclerotinia sclerotiorum* polygalacturonase enzymatic and necrotizing activities and delay symptoms in transgenic plants. *Can. J. Microbiol.* **59**, 79–86.

Brito, N., Espino, J.J. and Gonzalez, C. (2006) The endo-β-1,4-xylanase xyn11A is required for virulence in *Botrytis cinerea*. *Mol. Plant–Microbe Interact.* **19**, 25–32.

Cantu, D., Vicente, A.R., Labavitch, J.M., Bennett, A.B. and Powell, A.L.T. (2008) Strangers in the matrix: plant cell walls and pathogen susceptibility. *Trends Plant Sci.* **13**, 610–617.

Debyser, W., Peumans, W.J., Van Damme, E.J.M. and Delcour, J.A. (1999) *Triticum aestivum* xylanase inhibitor (TAXI), a new class of enzyme inhibitor affecting breadmaking performance. *J. Cereal Sci.* **30**, 39–43.

De Lorenzo, G., D'Ovidio, R. and Cervone, F. (2001) The role of polygacturonase-inhibiting proteins (PGIPs) in defense against pathogenic fungi. *Annu. Rev. Phytopathol.* **39**, 313–335.

Dornez, E., Croes, E., Gebruers, K., De Coninck, B., Cammue, B.P.A., Delcour, J.A. and Courtin, C.M. (2010) Accumulated evidence substantiates a role for three classes of wheat xylanase inhibitors in plant defense. *CRC Crit. Rev. Plant Sci.* **29**, 244–264.

Enkerli, J., Felix, G. and Boller, T. (1999) The enzymatic activity of fungal xylanase is not necessary for its elicitor activity. *Plant Physiol.* **121**, 391–397.

Faoro, F. and Iriti, M. (2005) Cell death behind invisible symptoms: early diagnosis of ozone injury. *Biol. Plant.* **49**, 585–592.

Fierens, E., Rombouts, S., Gebruers, K., Goesaert, H., Brijs, K., Beaugrand, J., Volckaert, G., Van Campenhout, S., Proost, P., Courtin, C.M. and Delcour, J.A. (2007) TLXI, a novel type of xylanase inhibitor from wheat (*Triticum aestivum*) belonging to the thaumatin family. *Biochem. J.* **403**, 583–591.

Furman-Matarasso, N., Cohen, E., Du, Q., Chejanovsky, N., Hanania, U. and Avni, A. (1999) A point mutation in the ethylene-inducing xylanase elicitor inhibits the β-1-4-endoxylanase activity but not the elicitation activity. *Plant Physiol.* **121**, 345–352.

Govrin, E.M. and Levine, A. (2000) The hypersensitive response facilitates plant infection by the necrotrophic pathogen *Botrytis cinerea*. *Curr. Biol.* **10**, 751–757.

Guyon, K., Balagué, C., Roby, D. and Raffaele, S. (2014) Secretome analysis reveals effector candidates associated with broad host range necrotrophy in the fungal plant pathogen *Sclerotinia sclerotiorum*. *BMC Genomics*, **15**, 336.

Hornak, V., Abel, R., Okur, A., Strockbine, B., Roitberg, A. and Simmerling, C. (2006) Comparison of multiple amber force fields and development of improved protein backbone parameters. *Proteins Struct. Funct.* **65**, 712–725.

Igawa, T., Ochiai-Fukuda, T., Takahashi-Ando, N., Ohsato, S., Takehico, S., Yamaguki, I. and Kimura, M. (2004) New TAXI-type xylanase inhibitor genes are inducible by pathogens and wounding in hexaploid wheat. *Plant Cell Physiol.* **45**, 1347–1360.

Iriti, M., Sironi, M., Gomarasca, S., Casazza, A.P., Soave, C. and Faoro, F. (2006) Cell death-mediated antiviral effect of chitosan in tobacco. *Plant Physiol. Biochem.* **44**, 893–900.

Labute, P. (2009) Protonate3D: assignment of ionization states and hydrogen coordinates to macromolecular structures. *Proteins Struct. Funct. Bioinf.* **75**, 187–205.

Livak, K.J. and Schmittgen, T.D. (2001) Analysis of relative gene expression data using Real-Time 17 quantitative PCR and 2–ΔΔCT method. *Methods*, **25**, 402–408.

Lu, S., Friesen, T.L. and Faris, J.D. (2011) Molecular characterization and genomic mapping of the pathogenesis-related protein 1 (PR-1) gene family in hexaploid wheat (*Triticum aestivum* L.). *Mol. Genet. Genomics*, **285**, 485–503.

Lu, Z.X., Gaudet, D., Puchalski, B., Despins, T., Frick, M. and Laroche, A. (2006) Inducers of resistance reduce common bunt infection in wheat seedlings while differentially regulating defence-gene expression. *Physiol. Mol. Plant Pathol.* **67**, 138–148.

McLauchlan, W.R., Garcia-Conesa, M.T., Williamson, G., Roza, M., Ravestein, P. and Maat, J. (1999) A novel class of protein from wheat which inhibits xylanases. *Biochem. J.* **338**, 441–446.

Moscetti, I., Tundo, S., Janni, M., Sella, L., Gazzetti, K., Tauzin, A., Giardina, T., Masci, S., Favaron, F. and D'Ovidio, R. (2013) Constitutive expression of the xylanase inhibitor TAXI-III delays Fusarium head blight symptoms in durum wheat transgenic plants. *Mol. Plant–Microbe Interact.* **26**, 1464–1472.

Noda, J., Brito, N. and González, C. (2010) The *Botrytis cinerea* xylanase Xyn11A contributes to virulence with its necrotizing activity, not with its catalytic activity. *BMC Plant Biol.* **10**, 38.

Pollet, A., Sansen, S., Raedschelders, G., Gebruers, K., Rabijns, A., Delcour, J.A. and Courtin, C.M. (2009) Identification of structural determinants for inhibition strength and specificity of wheat xylanase inhibitors TAXI-IA and TAXI-IIA. *FEBS J.* **276**, 3916–3927.

Ron, M. and Avni, A. (2004) The receptor for the fungal elicitor ethylene-inducing xylanase is a member of a resistance-like gene family in tomato. *Plant Cell*, **16**, 1604–1615.

Rotblat, B., Enshell-Seijffers, D., Gershoni, J.M., Schuster, S. and Avni, A. (2002) Identification of an essential component of the elicitation active site of the EIX protein elicitor. *Plant J.* **32**, 1049–1055.

Sella, L., Gazzetti, K., Faoro, F., Odorizzi, S., D'Ovidio, R., Schäfer, W. and Favaron, F. (2013) A *Fusarium graminearum* xylanase expressed during wheat infection is a necrotizing factor but is not essential for virulence. *Plant Physiol. Biochem.* **64**, 1–10.

Sharon, A., Fuchs, Y. and Anderson, J.D. (1993) The elicitation of ethylene biosynthesis by a *Trichoderma* xylanase is not related to the cell wall degradation activity of the enzyme. *Plant Physiol.* **102**, 1325–1329.

Wang, X., Tang, C., Zhang, H., Xu, J.R., Liu, B., Lv, J., Han, D., Huang, L. and Kang, Z. (2011) TaDAD2, a negative regulator of programmed cell death, is important for the interaction between wheat and the stripe rust fungus. *Mol. Plant–Microbe Interact.* **24**, 79–90.

Wang, X., Wang, X., Feng, H., Tang, C., Bai, P., Wei, G., Huang, L. and Kang, Z. (2012) TaMCA4, a novel wheat metacaspase gene functions in programmed cell death induced by the fungal pathogen *Puccinia striiformis* f. sp. *tritici*. *Mol. Plant–Microbe Interact.* **25**, 755–764.

Xin, Z., Wang, Q., Yu, Z., Hu, L., Li, J., Xiang, C., Wang, B. and Lou, Y. (2014) Overexpression of a xylanase inhibitor gene, *OsHI-XIP*, enhances resistance in rice to herbivores. *Plant Mol. Biol. Rep.* **32**, 465–475.

Zadoks, J.C., Chang, T.T. and Konzak, C.F. (1974) A decimal code for the growth stages of cereals. *Weed Res.* **14**, 415–421.

Zuppini, A., Navazio, L., Sella, L., Castiglioni, C., Favaron, F. and Mariani, P. (2005) An endopolygalacturonase from *Sclerotinia sclerotiorum* induces calcium-mediated signaling and programmed cell death in soybean cells. *Mol. Plant–Microbe Interact.* **18**, 849–855.

SUPPORTING INFORMATION

Additional Supporting Information may be found in the online version of this article at the publisher's website:

Fig. S1 Quantification of dead cells in lemmas of cv. Svevo treated with FGSG_03624 xylanase and TAXI-III.

Fig. S2 Quantification of dead cells in lemmas of cv. Svevo and transgenic TAXI-III plants.

Fig. S3 Overall structure of the homology modelling complexes of TAXI-III/xylanase FGSG_03624 generated starting from TAXI-I or TAXI-IIA.